Batteries & Supercaps

Chemistry Europe
European Chemical Societies Publishing

Accepted Article

Title: Exploring the possibility of aluminum plating/stripping from a non-corrosive Al(OTf)3-based electrolyte

Authors: Mahla Talari, Angelina Sarapulova, Eugen Zemlyanushin, Noha Sabi, Andreas Hofmann, Vanessa Trouillet, and Sonia Dsoke

To be cited as: *Batteries & Supercaps* **2024**, e202400317

Link to VoR: https://doi.org/10.1002/batt.202400317

WILEY VCH

10.1002/batt.202400317

Exploring the possibility of aluminum plating/stripping from a non-corrosive $Al(OTf)_3$-based electrolyte

Mahla Talari[a], Angelina Sarapulova[a,b,c], Eugen Zemlyanushin[a], Noha Sabi[a,d], Andreas Hofmann[a], Vanessa Trouillet[a], Sonia Dsoke[a,b,c,e*]

[a] *Institute for Applied Materials (IAM), Karlsruhe Institute of Technology (KIT), Hermann-von-Helmholtz-Platz 1, 76344 Eggenstein-Leopoldshafen, Germany*

[b] *FMF—Freiburg Materials Research Center, University of Freiburg, Stefan-Meier Str. 21, 79104 Freiburg, Germany*

[c] *Fraunhofer Institute for Solar Energy Systems, Dep. Electrical Energy Storage, Heidenhofstr. 2, 79110 Freiburg, Germany*

[d] *High Throughput Multidisciplinary Research (HTMR), Mohammed VI Polytechnic University, Lot 660 Hay Moulay Rachid, Ben Guerir, 43150, Morocco*

[e] *Institute for Sustainable Systems Engineering (INATECH), University of Freiburg, Emmy-Noether-Straße 2, 79110, Freiburg, Germany*

**Corresponding author: Sonia Dsoke (sonia.dsoke@ise.fraunhofer.de)*

Abstract

Rechargeable aluminum batteries offer a promising candidate for energy storage systems, due to the Aluminum (Al) abundance source. However, the development of non-corrosive electrolytes, facilitating reversible Al plating/stripping, is a critical challenge to overcome.

This study investigates the feasibility of aluminum plating on a platinum substrate using a non-corrosive trifluoromethanesulfonate ($Al(OTf)_3$)/*N*-methylacetamide (NMA)/urea electrolyte. This electrolyte was proposed earlier as an alternative chloroaluminate-based ionic liquid, but Al plating/stripping was not proved.

In this work, various techniques, including cyclic voltammetry, scanning electron microscope/energy-dispersive X-ray spectroscopy, *operando* optical microscopy and electrochemical quartz crystal microbalance (EQCM), gas chromatography (GC), and X-ray photoelectron spectroscopy were employed to understand the Aluminum plating and stripping behavior. While cyclic voltammetry indicates redox activity on Pt, further analysis reveals no significant plating. Instead, hydrogen evolution reaction, promoted by the water-residue, dominates the observed current, confirmed by *operando* microscopy and GC measurements. EQCM studies suggest the concurrent adsorption/desorption of $Al(OH)^{2+}$ and Al^{3+} ions on the Pt electrode.

Further drying the electrolyte reduces the hydrogen evolution, but plating of metallic Al remains elusive. These findings highlight the need for further optimization of the electrolyte composition to achieve efficient Al plating/stripping.

Keywords: Aluminum batteries, non-corrosive electrolyte, $Al(OTf)_3$-based electrolyte, Al plating, hydrogen evolution reaction.

Introduction

The transition from fossil fuels to renewables depends on efficient energy storage systems to address grid intermittency issues and provide energy storage for electrical applications.[2–4] Lithium-ion batteries (LIBs) are the most widely used electrochemical energy storage system due to lithium's (Li) lower reduction potential of -3.04 V *vs.* SHE (Standard Hydrogen Electrode) compared to other metals, which leads to the highest possible cell voltages.[5] LIBs exhibit high gravimetric/volumetric energy densities; however, the scarcity of Li resources as, as well as other typical components of cathode materials such as cobalt (Co) and nickel (Ni) in LIBs and their distribution in the earth's crust, major issues to meet the ever-demands for battery systems. [6–9] For this reason, researchers recognize the importance of developing other cell chemistries as alternatives to LIBs.[3,6,9–11] Among post-lithium candidates, sodium (Na), potassium (K), magnesium (Mg), aluminum (Al), calcium (Ca), and zinc (Zn)-ion batteries are of high interest.[12–23]Al abundant sources, along with the claim of the high theoretical volumetric capacity of Al as a metal anode, due to its trivalent nature, are advantageous of Al-based battery. [10,11,24] Additionally, Al offers sustainability and lower reactivity at ambient conditions, which results in safer handling, especially in situations involving accidental cell breakage. [3,4,9,11,25,26 27–29]

Nevertheless, to obtain a high-performance Al-based battery, an appropriate electrolyte that enables the reversible Al plating/stripping with high coulombic efficiency (CE) is crucial.[2,7,11,30] A major concern with such Al-based electrolytes is that the high charge density of the Al cation leads to strong coulombic interaction between Al cations and their counter anions, which negatively impacts the solvation behavior of Al salts. This means that conventional organic solvents may not be suitable.[1] Over the past decades, extensive research has been carried out to achieve Al plating/stripping in both aqueous and non-aqueous electrolytes, from early examples of molten salts to beyond liquid polymer electrolytes.[3,6,11,24,26–29,31,32]

Aqueous electrolytes have the advantages of being cost-efficient, non-flammable, and environmentally friendly.[8,33,34] However, several obstacles related to aqueous electrolytes hinder their use in Al batteries, including the risk of the hydrogen evolution reaction (HER) due to the lower equilibrium redox potential of Al (-1.66 V *vs.* SHE), revealing that the electrochemical stability window of the aqueous electrolyte is limited, making them unsuitable for the plating of Al.[8,33,35] Moreover, water molecules also facilitate the oxidation of the Al negative electrode to form the corrosion products such as $Al(OH)_4^-$ and $Al(OH)_3$.[8,34–36]

Non-aqueous electrolytes have been considered to overcome some of the problems associated with aqueous systems.[2,26,37,38] Room temperature ionic liquids (RTILs) electrolyte containing aluminum chloride salt ($AlCl_3$) and Lewis basic organic chlorides (A^+Cl^-, where A^+ represents an organic group such as 1-ethyl-3-methylimidazolium, 1-butyl-3-methylimidazolium and trimethylammonium) have been studied.[25,28,29,39] The advantages of RTILs are their high ionic conductivity, low vapor pressure, and wider electrochemical stability window compared to aqueous electrolytes, which enable Al plating.[26] Nevertheless, Al plating/stripping relies on an

10.1002/batt.202400317

optimized ratio between $AlCl_3$ and A^+Cl^- in the electrolyte composition. Within the molar ratio range of $AlCl_3$ to A^+Cl^- from 1 to 2, the "active" species of $Al_2Cl_7^-$ is responsible for the Al plating/stripping through **Eq.1** on the negative electrode.[40–42]

$$4\,Al_2Cl_7^- + 3e^- \rightleftharpoons Al + 7AlCl_4^- \qquad (Eq.1)$$

However, the higher the ratio of $AlCl_3$ to A^+Cl^-, the higher is desired active species, also the higher the Lewis acidity which leads to corrosion. This corrosion not only causes safety hazards but also escalates the difficulty of selecting compatible current collector materials and auxiliary parts of the battery.[7,8,25] Stainless steels, for example, exhibit severe corrosion, hindering the use of traditional coin cells (whose case is typically made of stainless steel).[7] Additionally, chloroaluminate-based electrolytes are highly sensitive to moisture, meaning that the formation of various electroactive spices, *e.g.*, hydrochloric acid (HCl) which is readily formed in the presence of moisture, can cause a safety concern.[6,25] An inert environment is therefore essential to prepare and handle the electrolytes, which limits and restricts the technological advancement of this cell chemistry.[1,43–45]

To replace corrosive $AlCl_3$, Aluminum bis(trifluoromethanesulfonyl) imide ($Al(TFSI)_3$) and aluminum trifluoromethane sulfonate ($Al(OTf)_3$) have been used in combination with different solvents, such as propylene carbonate (PC), tetrahydrofuran (THF) as well as 1-butyl-3-methylimidazolium trifluoromethane sulfonate ([BMIm]OTF) and even as „water-in-salt" aqueous electrolyte.[8,43,45–51]

T. Mandai and P. Johansson introduced a room-temperature (RT) ternary electrolyte composed of $Al(OTf)_3$, *N*- methylacetamide (NMA), and urea using the advantage of the entropic effect and the high solvation ability of the acetamide and urea mixture.[1] According to their study, the combination of the three components in the mole ratio of $Al(OTf)_3$/NMA/urea=0.05/0.76/0.19 shows the optimum physicochemical properties such as the high ionic conductivity (2.5 mS/cm, at 30 ºC) among several other molar ratios. This selection stems from the fact that while $Al(OTf)_3$ can form liquids with NMA/urea mixtures at ambient temperatures up to a 0.10 mole fraction of $Al(OTf)_3$, these liquids become excessively viscous, resulting in poor ionic conductivity.[1] In addition, the study provides important information on the changes in the dissociation state of $Al(OTf)_3$ with the different molar fractions of urea using Fourier Transformation-Infrared (FT-IR) and Raman spectroscopy.[1] This ternary electrolyte displays a wider electrochemical stability window, namely approximately 3.5 V, when compared to $AlCl_3$:EMImCl (aluminum chloride:1-ethyl-3-methylimidazolium chloride, ratio = 1.5 : 1, mol/mol, with a window of 2.3 V).[1] The reductive/oxidative currents obtained from the ternary electrolyte on the platinum (Pt) substrate have been correlated to Al plating/stripping.[1] Later on, the mechanism of dissociation of the $Al(OTf)_3$ in the NMA/urea mixture was studied using aluminum nuclear magnetic resonance spectroscopy (^{27}Al-NMR) and Raman spectroscopy revealing that Al complexes including $[AlOTf–solvent_x\text{-}urea_2]^{2+}$ are formed.[52] According to the suggestion of previous work, Al plating at the electrolyte/electrode interfaces is assumed to proceed through the desolvation of solvents and subsequent Al^{3+} reduction. The reverse reactions may occur during the stripping process.[1]

Although the physicochemical properties and dissociation mechanism of $Al(OTf)_3$ are well established, the Al plating from $Al(OTf)_3$/NMA/urea electrolyte is not yet proven and understood. This study aims to demonstrate the Al plating possibility and the impact of water

10.1002/batt.202400317

content due to the ineffective drying process of the electrolyte, by combining electrochemical techniques and analytical investigations such as SEM/EDX and EQCM analysis. Our results provide new insights into the side reactions taking place during the polarization, namely the hydrogen evolution reaction.

Experimental details and characterizations

Electrolyte preparation

Aluminum trifluoromethanesulfonate ($Al(OTf)_3$, 99.9%), *N*-methylacetamide (NMA, 99%), and urea (99%) were purchased from Sigma-Aldrich, Germany. According to the literature, all chemicals were dried under a vacuum at 80 ºC for 48 hours before the electrolyte preparation [1]. The electrolyte was prepared in an argon-filled glovebox (MBraun, <0.1 ppm H_2O and O_2). First, NMA was melted at 40 ºC, and then the appropriate amount of urea and $Al(OTf)_3$ were added to the solvent. The mixture was stirred using a magnetic bar at room temperature overnight, and the resulting ternary electrolyte of $Al(OTf)_3$/NMA/urea=0.05/0.76/0.19 (mole fraction) was used for measurements. The selection of this electrolyte molar ratio is based on a prior study by T. Mandai [1]. This study explored various molar ratios of the $Al(OTf)_3$/NMA/urea electrolyte systems to identify the composition with optimal physicochemical properties. Notably, $Al(OTf)_3$ miscibility with the NMA/urea mixture is limited to a maximum of 0.1 mole fraction, and the electrolyte formulated with a 0.1 mol fraction of $Al(OTf)_3$ exhibits extreme viscosity and poor ionic conductivity.

The electrolyte, prepared according to this method, which was outlined in the literature[1], contains more than 20000 ppm of water as measured by Karl Fisher (KF) titration. This electrolyte is referred to as ANU-20000 in this paper.

An additional drying step was implemented for the ANU-20000 electrolyte involving a four-month drying process using Calcium chloride ($CaCl_2$) and Phosphorus pentoxide (P_4O_{10}) as drying agents. These drying agents were not directly dispersed into the electrolyte, but the electrolyte was stored in the same container to prevent reactions with these chemicals. As a result, the water content was decreased to 300 ppm, as confirmed by Karl Fischer titration conducted within an argon-filled glovebox. The resulting dried electrolyte is designated as ANU-300.

In the case of urea-free electrolyte, the appropriate amount of $Al(OTf)_3$ was added to the melted NMA to achieve a 0.05 mole fraction of $Al(OTf)_3$ in NMA. Subsequently, the electrolyte was stirred overnight.

Karl Fisher (KF) titration was performed using SI Analytics Automatic titrator TitroLine® 7500 KF Trace for coulometric water determination. The KF titrator setup was calibrated with a 0.1% water standard (Honeywell International Inc., HYDRANAL Standard).

Electrochemical measurements

A TSC surface cell (rhd instruments, Germany) served as an air-tight three-electrode cell. It consisted of a Pt foil (99.95%, rhd instruments, Germany) as a working electrode, an Al wire as a pseudo-reference electrode (RE), and an Al disc counter electrode (CE). 800 µl of the electrolyte was used for each measurement conducted in this cell. Before any experiments, the Al and Pt electrodes were mechanically polished using diamond paste (0.25 µm), and the Al

10.1002/batt.202400317

wire pseudo-reference was chemically polished by immersion in a mixture of $H_2SO_4/H_3PO_4/HNO_3$ (25/70/5 by volume) for 15 minutes.

Cyclic voltammetry (CV) measurements were conducted using a multi-channel potentiostat/galvanostat (VMP3, Biologic Science Instrument GmbH, France) equipped with EC-Lab software, at room temperature. For the CV measurement, a potential window ranging from -1 V to 1.2 V *vs.* Al was scanned with a scan rate of 20 mV/s.

One aspect to consider is that the Al pseudo-reference is chosen under the assumption that the Al^{3+}/Al redox reaction is the equilibrium reaction on the reference. However, in this electrolyte, as the reduction of Al is not the dominant redox reaction, the measured potential is the difference between "the Pt equilibrium potential" and "the Al equilibrium potential". Consequently, using an Al wire as the pseudo-reference may not be an accurate choice in this particular situation. Interestingly, this aspect was not deemed problematic in earlier studies.

Thermal field emission scanning electron microscope (FE-SEM)

Surface morphology analysis was conducted by a thermal field emission scanning electron microscope (FE-SEM, Carl Zeiss SMT AG) at an acceleration voltage of 5.00 kV. The FE-SEM device is equipped with an energy-dispersive X-ray spectroscope (EDX, Quantax 400 SDD, Bruker). Chronoamperometry (CA) technique was applied by polarizing the Pt working electrode at -1 V *vs.* Al for 2 hours. The Pt electrode was washed with pure anhydrous methanol (MeOH) and dried for 30 min at room temperature under vacuum immediately after the measurement. The sample was fixed on a steel sample holder using sticky carbon tape.

Optical microscopy images

An optical cell called ECC-Opto-10 (EL-CELL, Germany) was used with the three-electrode cell setup of Al foils as counter and pseudo-reference electrodes and a Pt foil as a working electrode. Each measurement utilized 10 µl of electrolyte. During the CV measurement (operando), optical microscopy images were captured using a LEICA M205C microscope (Germany) while the CV measurement itself was conducted using a potentiostat/galvanostat (SP200, Biologic Science Instrument GmbH, France) equipped with EC-Lab software. The applied potentials ranged from -1 V to 1.2 V vs. Al, with a scan rate of 20 mV/s.

Gas chromatography (GC)

Gas chromatography (GC) was performed using a Clarus 690 GC (Perkin Elmer, USA) coupled to an ARNEL 4019 system (Perkin Elmer, USA) and mass spectroscopy (MS, SQ8S, Perkin Elmer, USA). The gas sample was taken *via* a self-made gas-tight connection from a TSC surface cell (rhd instruments, Germany, see supporting information, **Figure S1**) and introduced with a syringe into a loop system (Vici Valco) that was connected to various separation columns and injectors, namely a thermal conductivity detector (TCD) and a double TCD. The setup allowed the detection of the gases H_2, CO_2, CO, CH_4, C_2H_2, C_2H_4, C_2H_6, O_2, He, N_2, and Ar starting at a concentration of about 100 ppm. The gas samples were injected at room temperature and switched to the columns at normal pressure after the samples were depressurized. Evaluations were performed using TotalChrom 6.3.4 software (Perkin Elmer, USA) and Origin (OriginLab 2021). To increase the comparability between chromatograms, the intensities of TCD responses were normalized with respect to the peak area of Ar derived from the glovebox atmosphere.

10.1002/batt.202400317

Electrochemical quartz crystal microbalance (EQCM)

The air-protected QCM Flow Cell Kit (by Gamry Instruments) was used for EQCM measurement. The microbalance was set for a 5 MHz quartz crystal coated with Pt film on the working area of 1.1 cm². All experiments were conducted at room temperature using a quartz crystal coated with Pt as a working electrode, a wire of Al as the reference and an Al wire as counter electrodes. Pt-coated quartz crystal calibration was calibrated in a solution of $CuSO_4$ (5 mM) in 1 M H_2SO_4 before any measurement. The mass change at the working electrode was measured during cyclic voltammetry at the scan rate of 20 mV/s with an EQCM 10M combined with the Interface™ 1010 B Potentiostat/Galvanostat/ZRA (Gamry Instruments Inc, USA). The electrochemical test program includes several steps: 5 activation cycles in the potential region -0.6/1.2 V *vs.* Al, followed by 55 further cycles in the potential region -1.0/1.2 V *vs.* Al. However, as the Al pseudo reference experiences slight shifts during cycling,[53] the potential window was adjusted to maintain overpotential throughout the cycles.

The Sauerbrey method used to model the EQCM results and the theoretical details of this method are outlined in the Supplementary Information (SI). The influence of the gas formation on Sauerbrey equation validity was also estimated using the quality factor, which fluctuated within the range of $3*10^3$ to $6*10^3$. The quality factor (Q_E) is commonly defined as the ratio of the energy stored in the oscillation to the dissipated energy. It typically falls within the range of 10^3 to 10^6, when the surrounding environment does not dampen the oscillation. Q_E has been calculated with the Gamry software "Gamry Echem Analyst."

X-ray photoelectron spectroscopy (XPS)

XPS measurements were performed using a K-Alpha XPS spectrometer (ThermoFisher Scientific, UK) using a monochromated Al Kα X-ray source (400 μm spot size). Thermo Avantage software was used in data acquisition and processing. All spectra were referenced to the C 1s peak at 285.0 eV binding energy. The samples were placed on a sample holder in an Ar-filled glovebox connected to the spectrometer. Data acquisition and processing were carried out using the Thermo Avantage software (Version 5.9931, Thermo Scientific). All spectra were referenced to the hydrocarbon C 1s peak (C−C, C−H) at 285.0 eV. To provide a clear presentation and more comparable spectra, the intensity was normalized setting the maximum peak height to 1.

Samples preparation for XPS: The Chronoamperometry (CA) technique was applied by polarizing the Pt and copper (Cu) working electrode at -1 V *vs.* Al for 2 hours in the electrolyte containing 300 ppm of water. The Pt and Cu electrodes were washed with pure anhydrous methanol (MeOH) and dried for 30 min at room temperature under vacuum immediately after the measurement. An Al foil, with a purity of 99.0% (Goodfellow, USA) was used as a pristine sample.

Results and Discussions

Characterization of ANU-20000 Electrolyte: Literature-Based Preparation

10.1002/batt.202400317

CV was used to investigate the possibility of Al plating from the ANU-20000 electrolyte. **Figure 1** presents the voltammograms of the Pt electrode in the ANU-20000 electrolyte (0.05/0.76/0.19 in molar fraction) at a scan rate of 20 mV/s in the potential range between -1 V to 1.2 V *vs.* Al. The voltammograms reveal an oxidation peak at 0.35 V *vs.* Al and a reductive process that starts at around 0 V. Additionally, the same redox behavior can be observed within the cycles, showing the reproducibility of consecutive cycles. These reductive/oxidative currents were previously assigned to the Al plating/stripping along with possible electrolyte decomposition.[1]

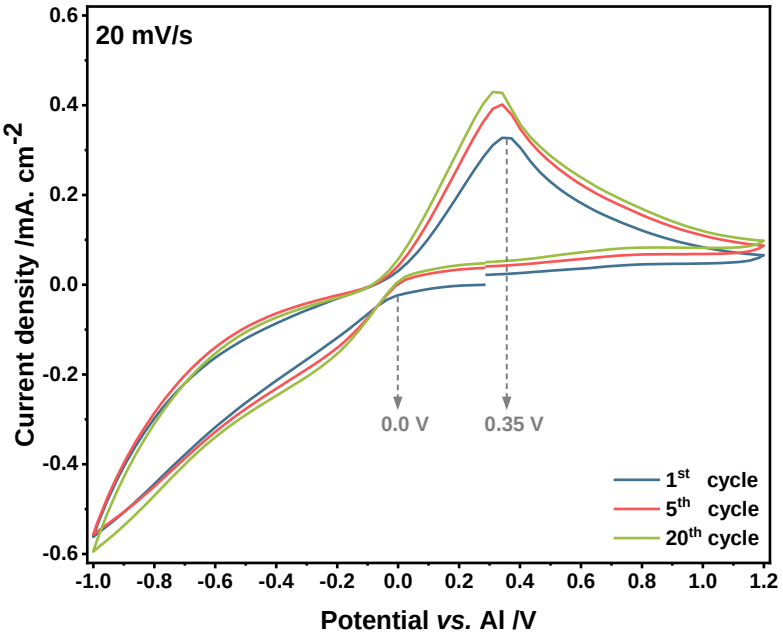

Figure 1. CV curves on the Pt working electrode in ANU-20000 electrolyte at a scan rate of 20 mV/s. Al were used as reference electrode and counter electrode.

To corroborate that the reduction current is due to Al plating, chronoamperometry (CA) by polarizing the Pt working electrode at -1 V *vs.* Al for 2 hours was applied, and then the Pt working electrode was investigated using field emission-scanning electron microscopy (FE-SEM) and energy-dispersive X-ray spectroscopy (EDX). The potential was chosen based on the work of T. Mandai and P. Johansson which has been mentioned that the reduction process starting at ~ -0.7 V *vs.* Al is supposed to be Al plating with a possible simultaneous decomposition of urea and NMA with bubbles formation on the Pt working electrode at ~ -1.2 V *vs.* Al.[15] To avoid side reactions at lower potentials, the potential of -1 V *vs.* Al was chosen.

In the experiments conducted with other electrolytes reported so far, such as $AlCl_3$:EMImCl at a molar ratio of 1:2 and $Al(OTf)_3$: $LiAlH_4$ at a 3:1 molar ratio in THF, the deposition of Al was detectable by FE-SEM and EDX.[45,54] However, no Al deposit can be detected on the Pt electrode surface with this non-corrosive electrolyte of ANU-20000 (**Figure 2).** See **Figure S2** for the corresponding EDX spectra.

10.1002/batt.202400317

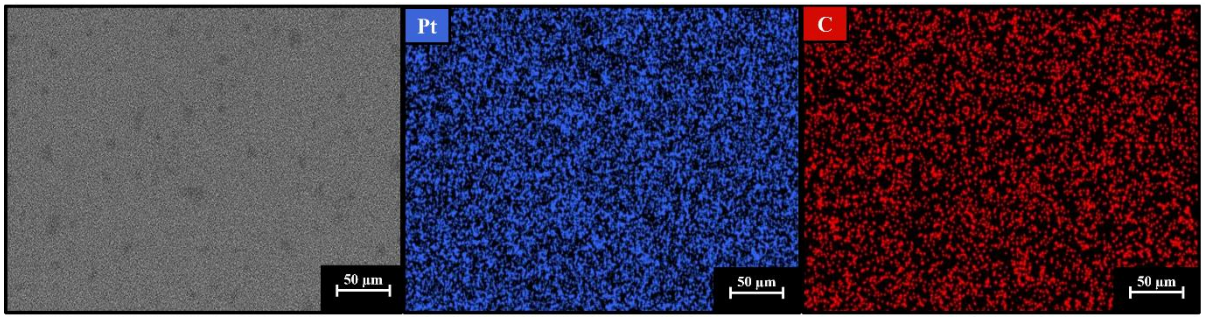

Figure 2. Field emission-scanning electron microscopy (FE-SEM) and energy-dispersive X-ray spectroscopy (EDX) images of the Pt working electrode polarized at -1 V *vs.* Al for 2 hours in ANU-20000 electrolyte.

The *operando* optical microscopy imaging of the Pt electrode was conducted to explore any optical/morphological change correlated to changes in potential. **Figure 3** shows the images of the Pt electrode taken at different potentials while measuring CV. It can be seen in **Figure 3** from points (a) to (d) that the formed gas bubbles (highlighted with a yellow-dashed circle) are reversibly growing and shrinking during the CV cycle. The reaction that leads to the formation of gas (points (a) to (c)) can be attributed to the hydrogen generated through the onset of hydrogen evolution (HER). The standard reduction potentials (E°) for HER is approximately 0 V *vs.* the standard hydrogen electrode (SHE), whereas the Al reduction ($Al^{+3} + \boldsymbol{e}^{-} \rightleftharpoons Al$) would be -1.66 V *vs.* SHE.[55] This implies that even under non-standard conditions (not at 25 ºC, 1 atm) and in non-aqueous electrolytes, the HER reaction can occur before Al reduction. The HER would point towards a considerable amount of water in the electrolyte. Indeed, despite strictly following the literature's guidelines,[1] including vacuum drying of all electrolyte components at 80 ºC, over 20,000 ppm of water remained, as measured using the Karl Fisher titration technique. This results in the formation of "stable gas pockets",[37] which may hinder the plating process of Al on Pt. Similar findings were also previously observed in the case of chromium[38] and nickel[39] plating. For a more detailed and visual understanding of the reversible gas formation on the Pt electrode during CV, a video demonstration is provided in the supporting information (**Video S1**).

10.1002/batt.202400317

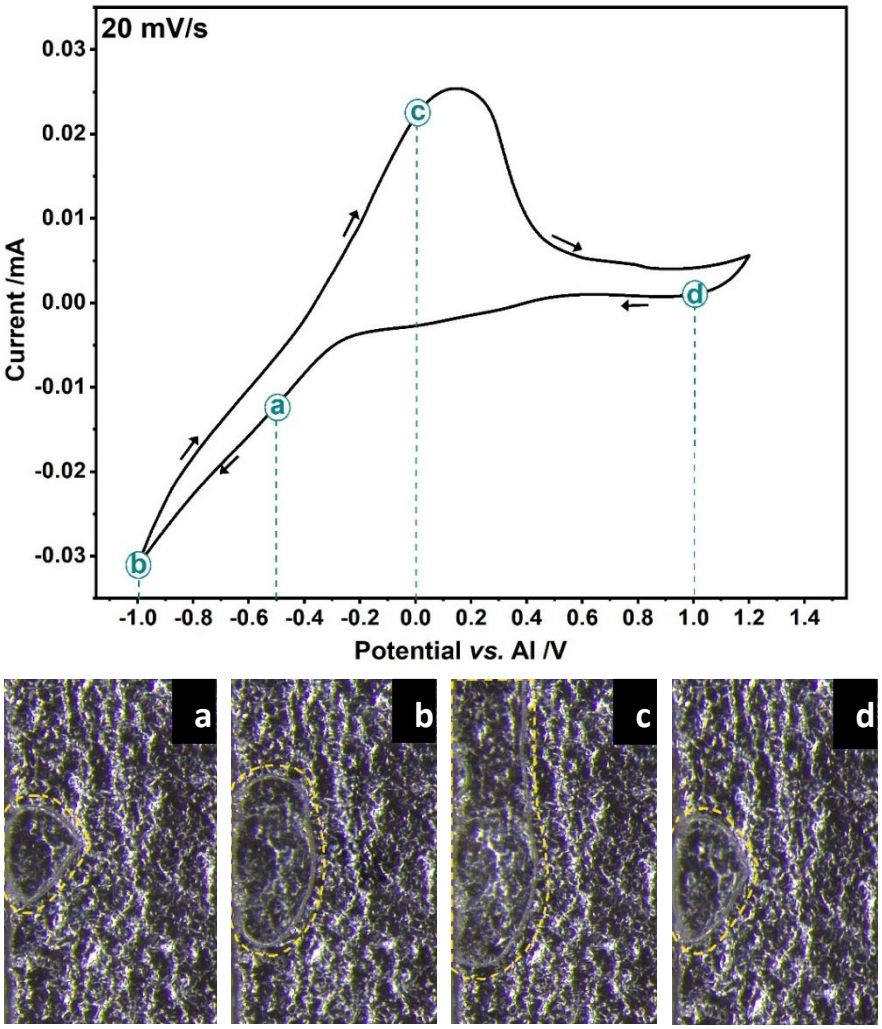

Figure 3. The Optical microscopy images of the Pt electrode captured during CV measurement in the potential window of -1 V to 1.2 V vs. Al at a scan rate of 20 mV/s in the ANU-20000 electrolyte. **(a)** -0.5 V *vs.* Al **(b)** -1 V *vs.* Al **(c)** 0 V *vs.* Al **(d)** 1 V *vs.* Al.

Gas chromatography (GC) analysis was performed to analyze the gases that are formed during polarization at negative potential. For this purpose, the Pt electrode was polarized at -1 V for 30 min in the ANU-20000 electrolyte, which was dried in the same way reported in the literature[1], and the resulting gas was collected in a gas-tight housing (TSC surface cell from rhd Instruments). This gas was then extracted with a syringe and injected into a GC. For the gas transfer, a tightly sealed connector was used (the gas-tight TSC surface cell is shown in **Figure S1**). **Figure 4 (a)** shows the chromatogram of the analyzed gas. The peak consisting of Ar and O_2, which could not be separated in the case of the chromatogram shown here, was separated in a second separation line, which considers only the Ar/O_2 separation. This shows that no oxygen was present, confirming the tightness of the cell and the appropriate gas transfer process (the cells were prepared under Ar inside the glovebox). The GC analysis reveals that the formed gas during the polarization of the Pt electrode is mainly nitrogen and hydrogen. No hydrogen can be observed in the "blank" chromatogram of the atmosphere of the glovebox, **Figure 4 (b).** Moreover, the nitrogen peak in **Figure 4 (a)** is significantly more pronounced than the one obtained in the blank. Therefore, based on these measurements it can be concluded that N_2 and H_2 gases are formed during the polarization of Pt in the ANU-20000 electrolyte.

10.1002/batt.202400317

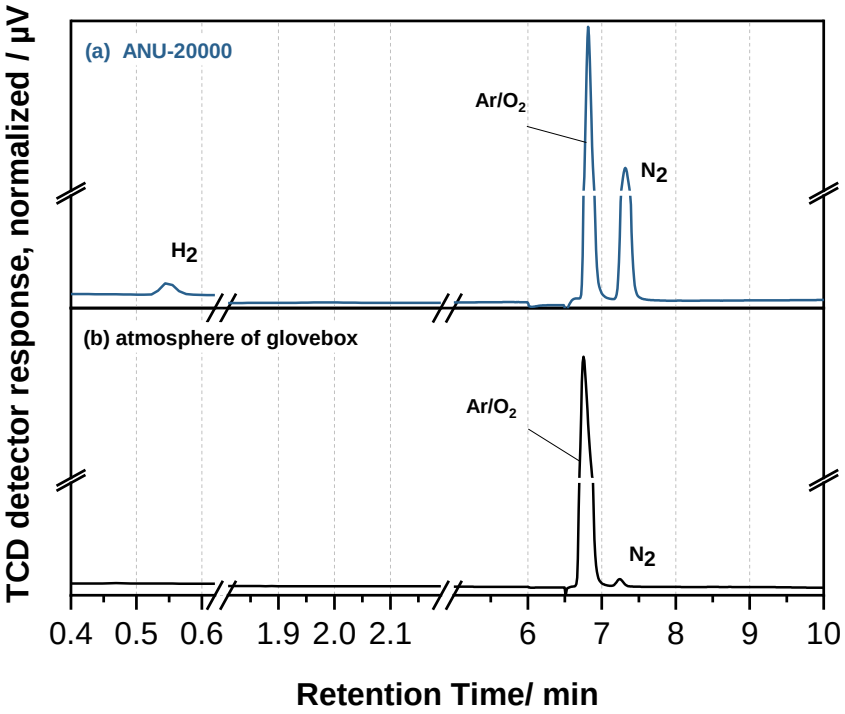

Figure 4. (a) GC spectrum of the collected gas after polarization of the Pt working electrode at -1 V vs. Al for 30 min in the ANU-20000 electrolyte (contains <20000 ppm of water) **(b)** GC spectrum of the collected gas from the atmosphere of the glovebox. The intensities of TCD responses are normalized with respect to the peak area of Ar from the glovebox atmosphere.

The Electrochemical gas migration mechanism investigated by GC may be supplemented by the EQCM technique, showing a mass of species that can be adsorbed on the working electrode. This helps us to model the electrochemical reactions on the interface of the Pt working electrode within the electrolyte. **Figure 5** shows electrode mass change vs. charge passed and potential *vs.* charge passed obtained from the EQCM measurement **(a)** of cycle 6th and **(b)** cycle 60th of the CV experiment. A cell with a 5 MHz Pt-coated quartz crystal working electrode and Al as a counter and reference electrode was used. A comparison is made between the 6th cycle and the 60th cycle to observe long-term cycling effects.

During the reduction process, HER can occur (previously confirmed by GC analysis), facilitated by hydrogen-bonded water molecules on the Pt surface in the ANU-20000 electrolyte.

As it is reported, under open circuit voltage (OCV) conditions in an acidic solution, a distinctive arrangement of hydrogen-bonded water molecules attached to the adsorbed hydroxyl groups on the Pt surface can be expected.[56] The initial step of HER (known as the Volmer step, **Eq.2**) involves the adsorption of hydrogen (H^*) onto the electrode surface. This process combines an electron transferred from a conductive substrate with a proton from a solution. However, in an alkaline solution, an additional prerequisite step of water dissociation is necessary before this reaction can occur, which may reduce the reaction rate.[57,58]

For the subsequent step, two possible reaction pathways have been generally accepted. This first pathway is the Heyrovsky reaction (**Eq.3**), where the adsorbed hydrogen atom combines with an electron and proton to form a hydrogen molecule, and the second pathway is the Tafel reaction (**Eq.4**), wherein two adjacent adsorbed hydrogen atoms combine to form a single hydrogen molecule (H_2). Free energies calculated by Density functional theory (DFT) highlight

10.1002/batt.202400317

the prevalence of the Volmer-Tafel route as the dominant mechanism over a wide range of pH.[43]

(Volmer) $$H_3O^+ + e^- + * \rightleftharpoons H^* + H_2O$$ *(Eq.2)*

(Heyrovsky) $$H_3O^+ + e^- + H^* \rightleftharpoons H_2 + H_2O$$ *(Eq.3)*

(Tafel) $$H^* + H^* \rightleftharpoons H_2$$ *(Eq.4)*

The HER mechanism model was combined with the model for reducing Al ions on the Pt surface, by incorporating EQCM measurements. Additionally, desorption of the hydroxyl groups can happen from the surface-active sites (*) together with a reduction of OH* to the OH^-. The formed Al^{3+} cations after dissociation of the solvated complex [AlOTf–$solvent_x$-$urea_2$]$^{2+}$ near the Pt surface react with the OH^- anions. The formation of $Al(OH)^{2+}$ complex ion on the Pt surface can play an important role in suppressing the Al plating from the proposed electrolyte.[59] Notably, the experimental mass change of the adsorbed species on the Pt surface during the reduction process at the 6th cycle is close to the molecular weight of the proposed formula of $Al(OH)^{2+}$ ions rather than the molecular weight of Al^{3+} ions. However, at the 60th cycle, the adsorption of Al^{3+} becomes more predominant in comparison to the adsorption of $Al(OH)^{2+}$ ions. The mathematically modeled molecular masses of active ions from the EQCM data suggest the concurrent adsorption of two species: $Al(OH)^{2+}$ and Al^{3+} ions on the Pt surface (**Figure 5 (a-b)**). Based on these assumptions, the proposed mechanism is illustrated in **Figure 5(c)**.

10.1002/batt.202400317

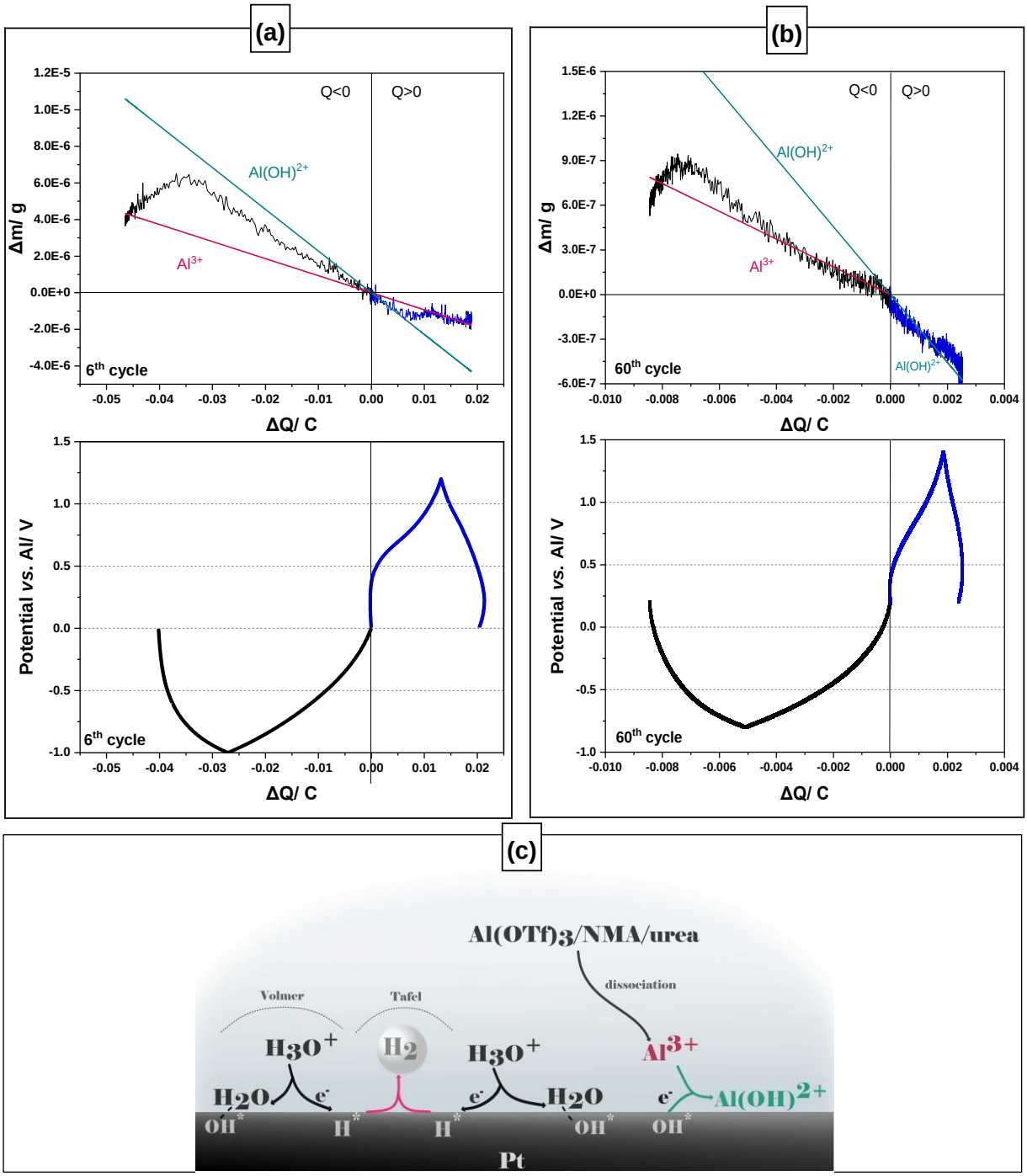

Figure 5. Electrode mass change *vs.* charge passed and potential *vs.* charge passed during CV measurement at scan rate of 20 mV/s on 5 MHz Pt-coated quartz crystal working electrode in the ANU-20000 electrolyte for cycles **(a)** 6th **(b)** 60th. Blue and black solid lines are measured mass change (EQCM), red and green lines are the theoretical mass change of neat ions calculated from Faraday's law. **(c)** The proposed mechanism.

The results of this study suggest that the hydrogen evolution reaction can coexist with Al solvating complex dissociation within the water-containing electrolyte near the Pt electrode surface. This implies that vacuum drying of the electrolyte at elevated temperatures, according

10.1002/batt.202400317

to literature,[1] is insufficient. $Al(OTf)_3$ salt, for instance, contains crystalline water, which cannot be removed by thermal desorption.[19]

The Impact of urea

To explore the possibility of nitrogen formation as a result of urea decomposition during the polarization, an electrolyte with the composition of $Al(OTf)_3$/NMA=0.05/0.95 (urea-free) was prepared for comparison. The Pt electrode was polarized under the same conditions at -1 V vs. Al for 1 hour in the urea-free electrolyte (see **Figure S3 (b)** for the GC spectrum of the collected gas). Comparative semiquantitative analysis of the GC spectra indicates a greater formation of nitrogen gas in the presence of urea, despite the shorter polarization time, underscoring urea's significant role in nitrogen formation. Moreover, the heightened hydrogen peak in the chromatogram for the urea-free electrolyte may be linked to the extended polarization duration.

Because the GC analysis demonstrates the influence of urea on N_2 gas formation in the electrolyte, further investigations were conducted to explore urea's effect on species adsorbing on the Pt surface during cyclic voltammetry (CV). EQCM results in the urea-free $Al(OTf)_3$/NMA electrolyte reveal less dissociation of $Al(OTf)_3$ salt, potentially leading to a more intense desorption process of OH^- species during reduction, with no cation adsorption observed. Consequently, the process becomes irreversible and results in no cation activity during subsequent oxidation (refer to **Figure S4**).

Combining the results from GC and EQCM analyses of the urea-free electrolyte, N_2 formation is likely linked to electrolyte decomposition, possibly occurring at the counter electrode. The counter electrode's potential (Al disc in the TSC surface cell) can exceed 3 V *vs.* Al during the measurements. It is important to highlight that when collecting the gas from the cell it is not possible to distinguish between gases generated at negative and positive electrodes. Therefore, precise identification of specific reactions involved in electrolyte decomposition and N_2 formation requires further investigation, beyond the scope of this research.

The Impact of Water Content

To emphasize the role of water content in the electrochemical reactions, we conducted supplementary experiments (CV, GC, and XPS) on an electrolyte with reduced water content. The electrolyte underwent a four-month drying process, using $CaCl_2$ and P_4O_{10} as drying agents. In this way, the water content of this electrolyte, labeled as ANU-300, was measured as 300 ppm, *via* Karl Fischer titration. It is crucial to highlight that the drying of such electrolyte composition is not so simple and difficult to apply in real systems because it requires such a long time.

Figure 6 illustrates the CV measurements of the Pt electrode conducted at a scan rate of 20 mV/s in the potential range between -1 V to 1.2 V *vs.* Al in the ANU-300 electrolyte compared with results obtained from electrolyte ANU-20000**.** The reductive/oxidative currents display a substantial reduction after the electrolyte drying process, unveiling a clear correlation between water content and current.

10.1002/batt.202400317

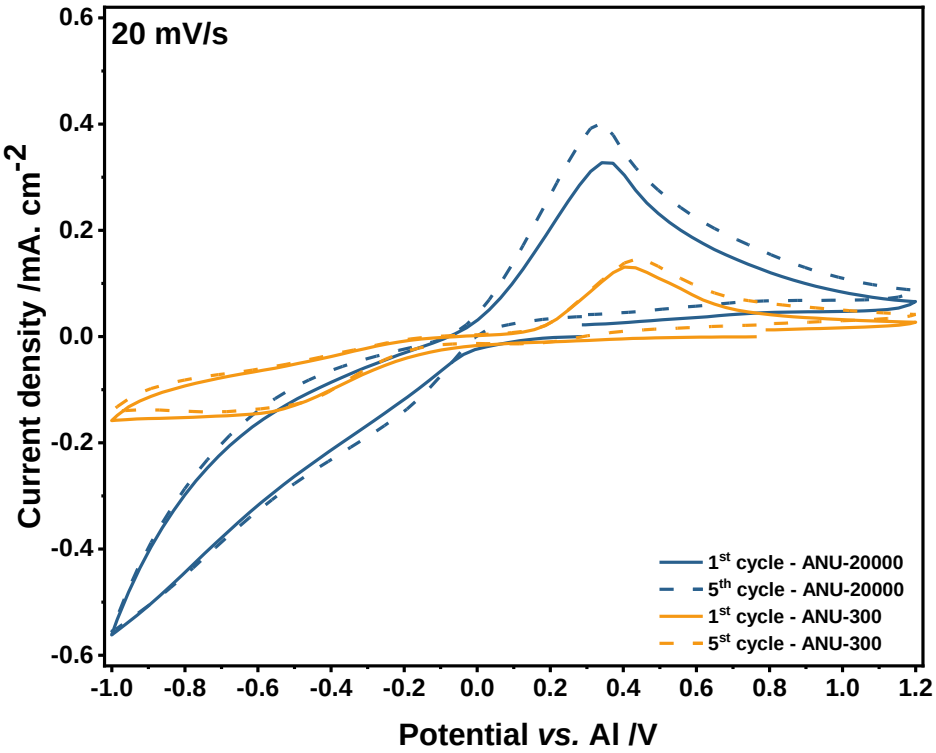

Figure 6. CV curves on the Pt working electrode in the ANU-20000 electrolyte (containing <20000 ppm of water) and the ANU-300 electrolyte (containing 300 ppm of water) at a scan rate of 20 mV/s. Al were used as reference electrode and counter.

To further validate the impact of water on the hydrogen evolution reaction (HER), GC analysis was conducted to assess the gases formed following the polarization of the Pt electrode at -1 V for 30 minutes in the ANU-300 electrolyte, as shown in **Figure 7 (b)**. This was compared with the GC measurement of the ANU-20000 electrolyte (**Figure 7(a)**). The gas produced during the 30 minutes was minimal, indicating a significant decrease in the hydrogen evolution reaction, with nearly undetectable hydrogen using the GC. N_2 was detected, possibly attributed to electrolyte decomposition. These measurements underscore that water is the predominant source of HER. Yet, a crucial question remains: does reducing the water content of the electrolyte facilitate meaningful Al plating?

To address this question, XPS characterization was employed to examine the presence of metallic Al on Pt surfaces after polarization at -1 V vs. Al for 2 hours in the ANU-300 electrolyte. It is noteworthy that the main photoelectron lines for Al and Pt, Al 2p and Pt 4f respectively, share the same binding energy range, hindering the investigation of eventual plated metallic Al solely through Al 2p (overlap). To overcome this, the Al 2s photoelectron line was utilized to determine the presence of metallic Al on the Pt electrode surface (**Figure 8 (a))** by comparison with the Al 2s spectrum of Al metal foil (**Figure 8 (b))** as a reference sample.

10.1002/batt.202400317

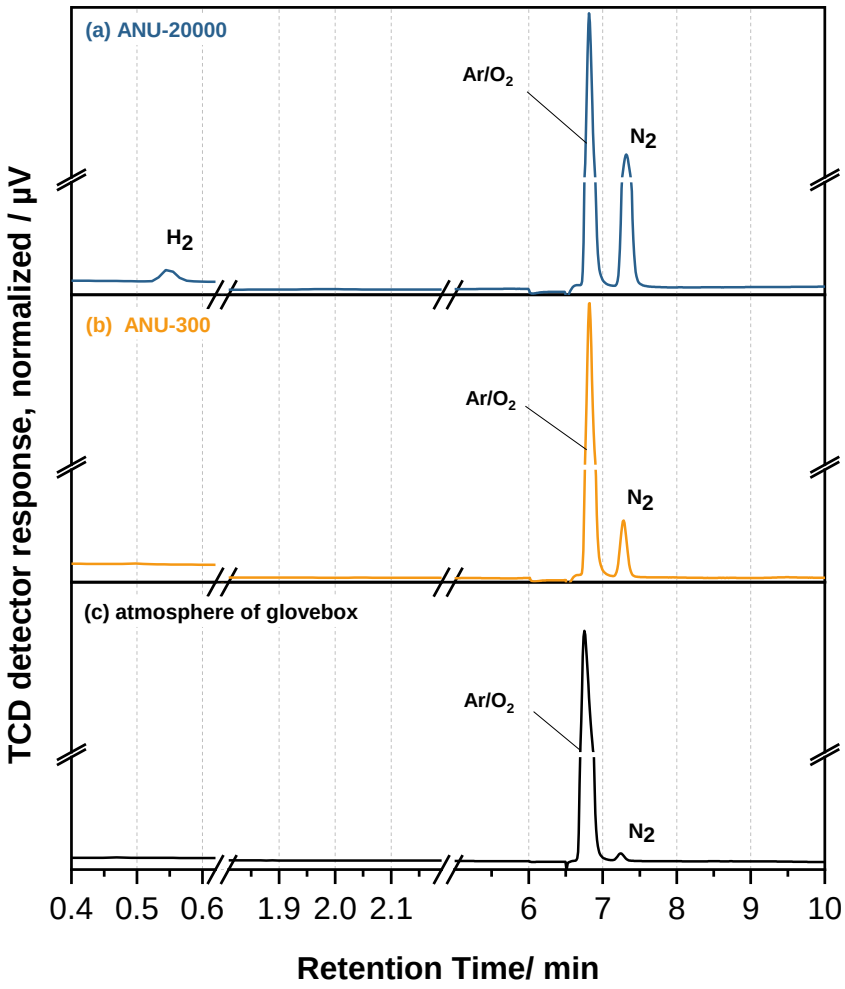

Figure 7. (a) GC spectrum of the collected gas after polarization of the Pt working electrode at -1 V *vs.* Al for 30 min in the ANU-2000 electrolyte (containing <20000 ppm of water). **(b)** GC spectrum of the collected gas after polarization of the Pt working electrode at -1 V *vs.* Al for 30 min in the ANU-300 electrolyte (containing 300 ppm of water) **(c)** GC spectrum of the collected gas from the atmosphere of the glovebox. The intensities of TCD responses are normalized with respect to the peak area of Ar from the glovebox atmosphere.

The Al 2s spectrum of Al metal foil exhibits two peaks at 116.5 eV and 119.6 eV, correlating to metallic Al (Al(0)) and Al native oxide (Al(III)) on the surface, respectively. The spectra of Al 2s for the Pt electrode were not fitted due to the low signal-to-noise ratio likely due to the very small amount of Al on the surface (near to the detection limit). However, upon comparing the Al 2s spectra of Al foil with those on Pt after polarization, the absence of metallic Al peak around 116.5 eV is evident. A small increase in the signal at around 120 eV is observed, potentially attributed to Al(III). This may be due to residue from the electrolyte remaining on the surface after washing with methanol. Unfortunately, even after reducing the water content, no plated Al could be identified using the experimental conditions applied. This absence could be attributed either to the small amount of plated Al, falling below the detection limit of the technique, or the difficulty of plating Al from this specific electrolyte. It is possible that residual water in the electrolyte still hinders Al plating on the Pt surfaces and/or the electrolyte composition is unsuitable for Al plating/stripping, potentially becasue the limited concentration of $Al(OTf)_3$ achievable due to its solubility constraints in the NMA/urea mixture.[1]

10.1002/batt.202400317

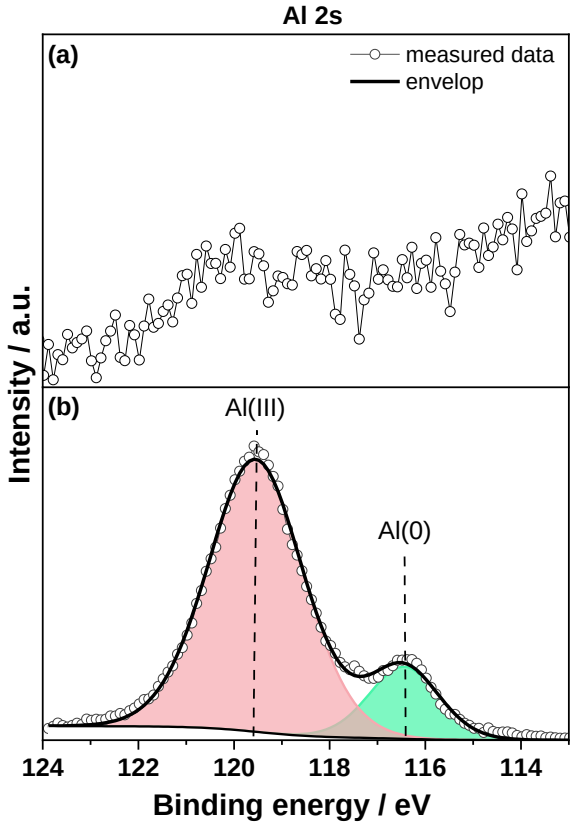

Figure 8. Al 2s spectra of **(a)** the Pt working electrode after polarization at -1 V *vs.* Al for 2 hours in the ANU-300 (containing 300 ppm water) and **(b)** Al metal foil.

To complement the study on the Pt electrode, XPS analysis was employed to investigate the possibility of Al plating onto a copper (Cu) substrate. The experiment mimicked the conditions used for the Pt working electrode, polarizing the Cu electrode at -1 V *vs.* Al for 2 hours in the ANU-300 electrolyte, followed by washing with methanol. The Al 2s spectra for Cu, alongside those of pure Al foil and Pt, are presented in **Figure S5**. The Al 2s spectrum of Cu allows for a direct comparison with the Al 2s spectra obtained from the Pt working electrode.

Comparing the Al 2s spectra of Al foil with those obtained with Pt and Cu after polarization reveals the absence of the metallic Al peak at around 116.5 eV for both Pt and Cu substrates. An increase in the signal around 120 eV and 122.4 eV could potentially be attributed to Al(III) from Al oxide/hydroxide that might have formed on the surface or residue from the electrolyte remaining after washing with methanol. Further investigation to identify the specific Al species present on the Cu surface is beyond the scope of this current research. However, the crucial observation is the lack of successful Al metal plating on the Cu surface using this electrolyte, even after extensive drying.

Conclusions

In this study, we have examined the possibility of Al plating on the Pt electrode from $Al(OTf)_3$/NMA/urea (ANU-20000) electrolyte in the molar fraction of 0.05/0.76/0.19, which is one of the previously proposed alternative to $AlCl_3$-based electrolytes. The results show the reductive/oxidative currents are mainly due to hydrogen evolution reactions as hydrogen gas

formation is observed and confirmed by the *operando* optical microscopy examination and GC measurement.

The EQCM study uncovered a mixed ion adsorption/desorption model for $Al(OH)^{2+}$ and Al^{3+} on the Pt surface during electrochemical CV measurements in the ANU-20000 electrolyte. The study confirms that the presence of urea facilitates the dissociation of the solvation molecules from the complex, leading to the preferable adsorption of Al^{3+} ions on the Pt electrode after 60 cycles. Despite the presence of adsorbed Al^{3+} ions on the Pt electrode, the occurrence of simultaneous side reactions limits the meaningful Al plating and stripping, as SEM analysis did not conclusively confirm the plating of Al from this electrolyte.

In the absence of urea, complete dissociation of $Al(OTf)_3$ salt does not occur, and no reversible adsorption process for the cations can be observed.

The water content in electrolytes, which remained through the literature-referenced drying method[1] is the primary responsible for the hydrogen evolution reaction (HER). A reduction in water content to 300 ppm notably decreases the reductive/oxidative currents and minimizes hydrogen evolution. However, under the tested conditions, metallic Al presence on Pt surfaces using XPS after polarization in the ANU-300 low-water electrolyte was not confirmed. The absence of Al plating in our experiments could be attributed to several factors. Firstly, the low concentration of metallic Al might fall below the detection limit of our technique. Secondly, residual water in the electrolyte may hinder the deposition of Al on the Pt surfaces. Lastly, it is possible that the composition of the electrolyte itself is not compatible with achieving successful Al plating or stripping. A potential contributor to this incompatibility could be the limited achievable concentration of $Al(OTf)_3$ due to its solubility limit within the NMA/urea mixture.

These findings emphasize the importance of optimizing electrolytes and identifying effective methods to eliminate water, advancing Al-based battery technologies beyond conventional chloroaluminate-based electrolytes.

Acknowledgments
The authors would like to thank Bettina Hunzinger for the SEM characterizations and Dr. David Rehnlund for his guidance and instruction on the optical microscopy cell used in this research. This work contributes to the research performed at CELEST (Center for Electrochemical Energy Storage Ulm-Karlsruhe) and was funded by the German Research Foundation (DFG) under Project ID 390874152 (POLiS Cluster of Excellence)

Data availability

The data that support the findings of this study are openly available at Zenodo with a DOI number of *10.5281/zenodo.10203292.*

Reference

1. Mandai, T. & Johansson, P. Al conductive haloaluminate-free non-aqueous room-temperature electrolytes. *J. Mater. Chem. A* **3**, 12230–12239 (2015).

2. Angell, M. *et al.* High Coulombic efficiency aluminum-ion battery using an AlCl3-urea ionic liquid analog electrolyte. *Proc. Natl. Acad. Sci.* **114**, 834–839 (2017).

3. Tu, J. *et al.* Nonaqueous rechargeable aluminum batteries: progresses, challenges, and perspectives. *Chem. Rev.* **121**, 4903–4961 (2021).

4. Ng, K. L., Lu, Z., Wang, Y., Singh, C. V. & Azimi, G. Fundamental insights into electrical and transport properties of chloroaluminate ionic liquids for aluminum-ion batteries. *J. Phys. Chem. C* **125**, 15145–15154 (2021).

5. Nitta, N., Wu, F., Lee, J. T. & Yushin, G. Li-ion battery materials: present and future. *Mater. today* **18**, 252–264 (2015).

6. Craig, B., Schoetz, T., Cruden, A. & de Leon, C. P. Review of current progress in non-aqueous aluminium batteries. *Renew. Sustain. Energy Rev.* **133**, 110100 (2020).

7. Zhang, Y., Liu, S., Ji, Y., Ma, J. & Yu, H. Emerging nonaqueous aluminum-ion batteries: challenges, status, and perspectives. *Adv. Mater.* **30**, 1706310 (2018).

8. Wu, X. *et al.* Reversible aluminum ion storage mechanism in Ti-deficient rutile titanium dioxide anode for aqueous aluminum-ion batteries. *Energy Storage Mater.* **37**, 619–627 (2021).

9. Schoetz, T. *et al.* Aluminium-poly (3, 4-ethylenedioxythiophene) rechargeable battery with ionic liquid electrolyte. *J. Energy Storage* **28**, 101176 (2020).

10. Ponrouch, A. *et al.* Multivalent rechargeable batteries. *Energy Storage Mater.* **20**, 253–262 (2019).

11. Han, X. *et al.* Electrolytes for Rechargeable Aluminum Batteries. *Prog. Mater. Sci.* 100960 (2022).

12. Cheng, Y. *et al.* Highly reversible zinc-ion intercalation into chevrel phase Mo6S8 nanocubes and applications for advanced zinc-ion batteries. *ACS Appl. Mater. Interfaces* **8**, 13673–13677 (2016).

13. Kummer, J. T. & Weber, N. A sodium-sulfur secondary battery. *Sae Trans.* 1003–1028 (1968).

14. Ponrouch, A., Frontera, C., Bardé, F. & Palacín, M. R. Towards a calcium-based rechargeable battery. *Nat. Mater.* **15**, 169–172 (2016).

15. Martinez-Cisneros, C. S. *et al.* Opening the door to liquid-free polymer electrolytes for calcium batteries. *Electrochim. Acta* **353**, 136525 (2020).

16. Chandrasekaran, R., Ruth Mangani, I., Vasanthi, R. & Selladurai, S. Ionic conductivity and battery characteristic studies on PEO+ NaClO 3 polymer electrolyte. *Ionics (Kiel).* **7**, 88–93 (2001).

17. Singer, J., Fielder, W. L., Kautz, H. E. & Fordyce, J. S. New solid conductors of Na+ and K+ ions. *J. Electrochem. Soc.* **123**, 614 (1976).

18. Zhao, Q., Hu, Y., Zhang, K. & Chen, J. Potassium–sulfur batteries: A new member of room-temperature rechargeable metal–sulfur batteries. *Inorg. Chem.* **53**, 9000–9005 (2014).

19. Di Noto, V., Lavina, S., Longo, D. & Vidali, M. A novel electrolytic complex based on δ-MgCl2 and poly (ethylene glycol) 400. *Electrochim. Acta* **43**, 1225–1237 (1998).

20. Di Noto, V., Münchow, V., Vittadello, M., Collet, J. C. & Lavina, S. Synthesis,

characterization and conductivity studies of Li and Mg polymer electrolytes based on esters of ethylenediaminetetraacetic acid and PEG400. *Solid State Ionics* **147**, 397–402 (2002).

21. Biscazzo, S., Vittadello, M., Lavina, S. & Di Noto, V. Synthesis and structure of electrolytic complexes based on α-hydro-ω-oligo (oxyethylene) hydroxy-poly [oligo (oxyethylene) oxydimethylsililene] and δ-MgCl2. *Solid state ionics* **147**, 377–382 (2002).

22. Dominko, R. *et al.* Magnesium batteries: Current picture and missing pieces of the puzzle. *J. Power Sources* **478**, 229027 (2020).

23. Lipson, A. L. *et al.* Rechargeable Ca-ion batteries: a new energy storage system. *Chem. Mater.* **27**, 8442–8447 (2015).

24. Das, S. K., Mahapatra, S. & Lahan, H. Aluminium-ion batteries: developments and challenges. *J. Mater. Chem. A* **5**, 6347–6367 (2017).

25. Muñoz-Torrero, D., Palma, J., Marcilla, R. & Ventosa, E. A critical perspective on rechargeable Al-ion battery technology. *Dalt. Trans.* **48**, 9906–9911 (2019).

26. Yuan, D., Zhao, J., Manalastas Jr, W., Kumar, S. & Srinivasan, M. Emerging rechargeable aqueous aluminum ion battery: Status, challenges, and outlooks. *Nano Mater. Sci.* **2**, 248–263 (2020).

27. Pagot, G., Vezzù, K., Greenbaum, S. G. & Di Noto, V. Hybrid twin-metal aluminum–magnesium electrolytes for rechargeable batteries. *J. Power Sources* **493**, 229681 (2021).

28. Zhu, G. *et al.* Rechargeable aluminum batteries: effects of cations in ionic liquid electrolytes. *RSC Adv.* **9**, 11322–11330 (2019).

29. Xu, H. *et al.* Low-cost AlCl3/Et3NHCl electrolyte for high-performance aluminum-ion battery. *Energy Storage Mater.* **17**, 38–45 (2019).

30. Reed, L. D., Arteaga, A. & Menke, E. J. A combined experimental and computational study of an aluminum triflate/diglyme electrolyte. *J. Phys. Chem. B* **119**, 12677–12681 (2015).

31. Schötz, T., de Leon, C. P., Ueda, M. & Bund, A. Perspective—state of the art of rechargeable aluminum batteries in non-aqueous systems. *J. Electrochem. Soc.* **164**, A3499 (2017).

32. Leung, O. M., Schoetz, T., Prodromakis, T. & Ponce de Leon, C. Review—Progress in Electrolytes for Rechargeable Aluminium Batteries. *J. Electrochem. Soc.* **168**, 056509 (2021).

33. Pastel, G. R. *et al.* A sobering examination of the feasibility of aqueous aluminum batteries. *Energy Environ. Sci.* (2022).

34. Li, Q. & Bjerrum, N. J. Aluminum as anode for energy storage and conversion: a review. *J. Power Sources* **110**, 1–10 (2002).

35. Dong, T., Ng, K. L., Wang, Y., Voznyy, O. & Azimi, G. Solid electrolyte interphase engineering for aqueous aluminum metal batteries: a critical evaluation. *Adv. Energy Mater.* **11**, 2100077 (2021).

36. Egan, D. R. *et al.* Developments in electrode materials and electrolytes for aluminium–air batteries. *J. Power Sources* **236**, 293–310 (2013).

37. Agiorgousis, M. L., Sun, Y.-Y. & Zhang, S. The role of ionic liquid electrolyte in an aluminum–graphite electrochemical cell. *ACS Energy Lett.* **2**, 689–693 (2017).

38. Huynh, T.-C., Dao, Q. P. D., Truong, T.-N., Doan, N.-G. & Ho, S.-L. Electrodeposition of aluminum on cathodes in ionic liquid based choline chloride/urea/AlCl3. *Environ. Pollut* **3**, 59–69 (2014).

39. Wang, H. *et al.* Anion-effects on electrochemical properties of ionic liquid electrolytes for rechargeable aluminum batteries. *J. Mater. Chem. A* **3**, 22677–22686 (2015).

40. Reynolds, G. F. & Dymek Jr, C. J. Primary and secondary room temperature molten salt electrochemical cells. *J. Power Sources* **15**, 109–118 (1985).

41. Qin, Q.-X. & Skyllas-Kazacos, M. Electrodeposition and dissolution of aluminium in ambient temperature molten salt system aluminium chloride n-butylpyridinium chloride. *J. Electroanal. Chem. Interfacial Electrochem.* **168**, 193–206 (1984).

42. Dymek, C. J., Williams, J. L., Groeger, D. J. & Auborn, J. J. An aluminum acid-base concentration cell using room temperature chloroaluminate ionic liquids. *J. Electrochem. Soc.* **131**, 2887 (1984).

43. Chiku, M., Matsumura, S., Takeda, H., Higuchi, E. & Inoue, H. Aluminum bis (trifluoromethanesulfonyl) imide as a chloride-free electrolyte for rechargeable aluminum batteries. *J. Electrochem. Soc.* **164**, A1841 (2017).

44. Terada, S. *et al.* Dissociation and Diffusion of Glyme-Sodium Bis(trifluoromethanesulfonyl)amide Complexes in Hydrofluoroether-Based Electrolytes for Sodium Batteries. *J. Phys. Chem. C* **120**, 23339–23350 (2016).

45. Slim, Z. & Menke, E. Hydride-Enhanced Plating and Stripping of Aluminum from Tri-flate-Based Organic Electrolytes. (2022).

46. Slim, Z. & Menke, E. J. Comparing Computational Predictions and Experimental Results for Aluminum Triflate in Tetrahydrofuran. *J. Phys. Chem. B* **124**, 5002–5008 (2020).

47. Mandai, T., Masu, H. & Johansson, P. Extraordinary aluminum coordination in a novel homometallic double complex salt. *Dalt. Trans.* **44**, 11259–11263 (2015).

48. Slim, Z. & Menke, E. J. Aluminum Electrodeposition from Chloride-Rich and Chloride-Free Organic Electrolytes. *J. Phys. Chem. C* **126**, 2365–2373 (2022).

49. Pan, W. *et al.* A low-cost and dendrite-free rechargeable aluminium-ion battery with superior performance. *J. Mater. Chem. A* **7**, 17420–17425 (2019).

50. Wang, H. *et al.* High-voltage and noncorrosive ionic liquid electrolyte used in rechargeable aluminum battery. *ACS Appl. Mater. Interfaces* **8**, 27444–27448 (2016).

51. Ejigu, A. *et al.* Optimization of Electrolytes for High-Performance Aqueous Aluminum-Ion Batteries. *ACS Appl. Mater. Interfaces* (2022).

52. Peters, W., Duong, H. T., Lee, S. & Drillet, J.-F. Investigation of Al (TfO) 3-based deep eutectic solvent electrolytes for aluminium-ion batteries. Part I: understanding the positively charged Al complex formation. *Phys. Chem. Chem. Phys.* **23**, 21923–21933

(2021).

53. Rahide, F. Open Challenges on Aluminum Triflate-Based Electrolytes for Aluminum Batteries Open Challenges on Aluminum Tri fl ate-Based Electrolytes for Aluminum Batteries. (2023) doi:10.1149/1945-7111/acc762.

54. Tang, J. & Azumi, K. Optimization of pulsed electrodeposition of aluminum from AlCl3-1-ethyl-3-methylimidazolium chloride ionic liquid. *Electrochim. Acta* **56**, 1130–1137 (2011).

55. Lide, D. R. *CRC handbook of chemistry and physics*. vol. 85 (CRC press, 2004).

56. Di Liberto, G. & Giordano, L. Role of solvation model on the stability of oxygenates on Pt (111): A comparison between microsolvation, extended bilayer, and extended metal/water interface. *Electrochem. Sci. Adv.* e2100204 (2023).

57. Skúlason, E. *et al.* Modeling the Electrochemical Hydrogen Oxidation and Evolution Reactions based on Density Functional Theory Calculations. *J. Phys. Chem. C* **114**, 18182–18197 (2010).

58. Liu, L., Liu, Y. & Liu, C. Enhancing the Understanding of Hydrogen Evolution and Oxidation Reactions on Pt(111) through Ab Initio Simulation of Electrode/Electrolyte Kinetics. *J. Am. Chem. Soc.* **142**, 4985–4989 (2020).

59. Lee, S. S., Schmidt, M., Sturchio, N. C., Nagy, K. L. & Fenter, P. Effect of pH on the formation of gibbsite-layer films at the muscovite (001)–water interface. *J. Phys. Chem. C* **123**, 6560–6571 (2019).